Structural Determination of the O-Chain Moieties of the Lipopolysaccharide Fraction from *Agrobacterium radiobacter* DSM 30147

Cristina De Castro,*[a] Emiliano Bedini,[a] Domenico Garozzo,[b] Luisa Sturiale,[b] and Michelangelo Parrilli[a]

Keywords: Agrobacterium / Conformational analysis / Lipopolysaccharide / NMR spectroscopy / Structure determination

Two O-chain structures were identified after acid hydrolysis of the lipopolysaccharide fraction of *Agrobacterium radiobacter* (type strain). The first is constituted by the linear tetrasaccharide repeating unit [2)-α-L-Rha*p*-(1→3)-α-L-Rha*p*-(1→3)-α-L-Rha*p*-(1→2)-α-L-Rha*p*-(1→]$_n$ and the second by the (1→2)-branched repeating unit α-D-Man*p*-(1→2)–[3)-α-D-Fuc*p*-(1→3)-α-D-Fuc*p*-(1→]$_n$.The two structures were determined mainly by 1D- and 2D NMR spectroscopy together with chemical-degradation methods. A detailed analysis of the NOESY spectrum, supported by molecular dynamics calculations, suggested that some unexpected NOEs were due to the sum of many small dipolar effects, whose identification was possible only by considering the 3D structure of an O-chain oligosaccharide bigger than the repeating unit.

Introduction

The *Agrobacterium* genus contains several phytopathogenic species such as *tumefaciens*, *rhizogenes* and *vitis*. All these soil Gram-negative bacteria exhibit several similarities at the chromosomal level and their pathogenic activity is generally linked to the plasmidic DNA. In the case of *A. tumefaciens* the bacterium−plant interaction leads to a complex series of events terminating in the insertion of a portion of the bacterial T_i plasmid into the plant-cell DNA, the mutated cells grow abnormally and the resulting disease is called crown gall tumour.

In this context, *Agrobacterium radiobacter* gains its importance since it is not able to carry the plasmidic DNA and it is not phytopathogenic at all.[1] In addition, it competes with *A. tumefaciens* for food and space on the plant cell wall. For these reasons, some strains of *A. radiobacter*, such as k84 or the genetically modified k1026 for instance, are sold as bio-pesticides.[2]

The importance of *radiobacter* is connected with its ability to adsorb on the plant cell walls, protecting all the potential infecting sites from the harmful activity of *A. tumefaciens*. This recognition and adhesion process is mediated by the components of the external bacterial membrane — both the proteins and the lipopolysaccharides (LPSs).[3,4] Despite the wealth of information about the biological role of the LPS components, in the case of *Agrobacterium* species, only a few data are available on their chemical structures.[5−8] In the framework of our investigation on the structure of the LPSs from *Agrobacterium* species we now report the structural elucidation of the LPS O-chains from *A. radiobacter* (type strain). This investigation is even more interesting since recent reports describe the involvement of *A. radiobacter* strains in human infections.[9,10]

Results and Discussion

The freeze-dried bacterial cells, after sequential washing with ethanol, acetone and diethyl ether, were extracted with a mixture of phenol/chloroform/petroleum ether (PCP method),[11] to give the LPS-1 fraction. The solid residue left after PCP extraction was treated with a mixture of phenol/water, according to Westphal and Jann,[12] yielding the fractions LPS-2 and LPS-3 from the phenol and the aqueous phase, respectively. The electrophoretic analysis of these fractions (results not shown) showed that LPS-1 and LPS-3 were S-form lipopolysaccharides whereas LPS-2, which was discarded, contained only lipooligosaccharides. The monosaccharide analysis of the LPS-1 and LPS-3 fractions showed, in both cases, the presence of rhamnose, fucose, mannose, glucose and traces of ribose, galactose, glucosamine and kdo. These latter sugars were attributed as being due to core and lipid A moieties and to nucleic acid impurities. In addition, the glucose was very abundant only in the LPS-3 fraction due to the presence of cyclic glucans, which were removed by gel chromatography. As for the gly-

[a] Dipartimento di Chimica Organica e Biochimica, Università di Napoli, Complesso Universitario Monte Sant′ Angelo, Via Cintia 4, 80126 Napoli, Italy
Fax: + 39-081-674-393
E-mail: decastro@unina.it
[b] Istituto di Chimica e Tecnologia dei Polimeri, CNR Viale R. Margherita 6, 95123 Catania, Italy
Fax: + 39-095-442-978

  DOI: 10.1002/ejoc.200400238

cosylation points of each residue, the methylation analysis of the LPS-1 and the purified LPS-3 fractions indicated the presence, as major components, of 2- and 3-linked rhamnose, 3- and 2,3-linked fucose and terminal-mannose units. The lipid analysis of both the LPS fractions revealed the presence of C-14:0 (3OH), C-16:0 and C18:0 fatty-acid residues. The absolute configurations of the pertinent monosaccharides, obtained by GLC analysis of the 2-octyl glycosides, were L for rhamnose and D for fucose and mannose.

At this point, owing to the identity of the two LPS fractions, further investigation was performed only on the more abundant purified LPS-3 fraction. Lipid-A was cleaved from the LPS fraction by mild acetic acid hydrolysis and separated by centrifugation; the supernatant was chromatographed on Sephacryl HR-100 and resolved in five peaks (Figure 1): the first (A) was attributed to unchanged LPS material, B and C were assigned to the O-chain and D and E to oligosaccharides of the core moieties. In order to see if the peaks B and C were representative of two chemically different O-chains or only of two different sizes of the same O-chain, the chromatographic fractions were pooled, dividing each peak into two halves. The four fractions obtained were named B1, B2, C1 and C2 according to the decrease of their molecular mass values. A comparison of the anomeric signal intensities in their ^{1}H NMR spectra (see a−d in Figure 2) suggested the presence of two chemically distinct O-chains, in particular the two anomeric signals A and C are more intense in Figure 2 (a) than in Figure 2 (d), whereas the opposite occurred for the signals E, F, and G, which are more intense in Figure 2 (d). In addition, the intensity of the signal at δ = 5.04 ppm apparently does not change on going from a to d in Figure 2, probably due to the overlapping of the two distinct anomeric signals, B and D, each of them associated with a different O-chain.

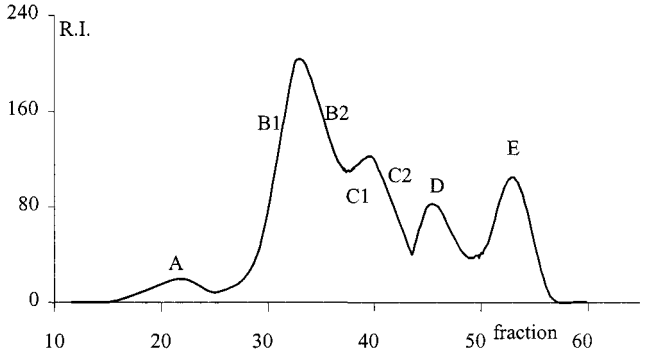

Figure 1. Sephacryl HR 100 purification of O-chain mixture

All the chromatographic efforts to separate these O-chains by low-pressure chromatography failed, and consequently the NMR spectroscopic investigation was accomplished directly on the mixture. Complete assignment of ^{1}H and ^{13}C resonances was achieved (Table 1) starting from the signals of the anomeric nuclei by DQ-COSY, TOCSY, NOESY, and HSQC 2D NMR experiments. The rhamnose residues, labelled as D, E, F and G, were easily

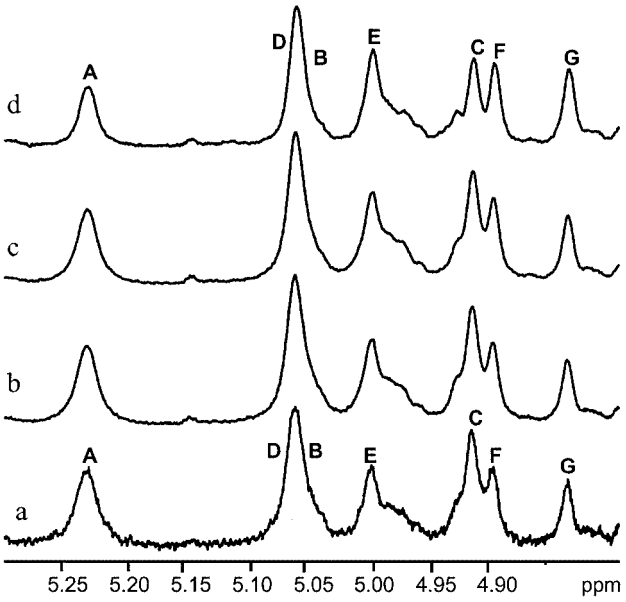

Figure 2. ^{1}H NMR (500 MHz) spectra of anomeric regions of fractions: (a) B1, (b) B2, (c) C1 and (d) C2 derived from Sephacryl HR 100 purification

Table 1. ^{1}H and ^{13}C (italic) chemical shifts of the two O-chains with repeating units ABC and DEFG, respectively, at 500 MHz (D_2O, 25 °C), of *A. radiobacter* DSM 30147

		1	2	3	4	5	6
A	2,3-α-D-Fuc*p*	5.35	4.17	4.21	4.15	4.33	1.25
		92.5	*68.2*	*72.5*	*67.9*	*66.9*	*16.5*
B	3-α-D-Fuc*p*	5.18	3.97	3.97	4.03	4.27	1.28
		94.9	*66.6*	*75.5*	*69.00*	*67.1*	*16.5*
C	*t*-α-D-Man*p*	5.04	3.94	3.70	3.62	3.83	3.74−4.01
		96.2	*70.0*	*70.4*	*67.0*	*72.6*	*61.5*
D	2-α-L-Rha*p*	5.18	4.08	3.96	3.50	3.85	1.31
		101.1	*78.3*	*70.0*	*72.4*	*69.5*	*17.6*
E	2-α-L-Rha*p*	5.12	4.10	3.91	3.49	3.73	1.28
		101.6	*78.3*	*70.0*	*72.4*	*69.5*	*17.6*
F	3-α-L-Rha*p*	5.02	4.13	3.91	3.57	3.89	1.31
		102.5	*70.1*	*78.5*	*71.8*	*69.8*	*17.7*
G	3-α-L-Rha*p*	4.96	4.17	3.84	3.55	3.77	1.28
		102.2	*70.1*	*78.3*	*71.8*	*69.8*	*17.7*

recognised by exploiting the coupling-constant information contained in the DQ-COSY spectrum. The shape of the H-3/H-2 cross peak (see a in Figure 3) was also very informative: it showed a small, active $^3J_{H2,H3}$ coupling and a large, passive one with proton H-4, whereas the H-4/H-3 cross peak contained only the boundary densities due to the large and equivalent coupling constant values of $^3J_{H4,H3}$ and $^3J_{H4,H5}$ (see b in Figure 3).

Information regarding the substitution pattern of the rhamnose moieties was obtained by analysis of the NOESY spectrum (Figure 4); the following dipolar couplings were attributed: H-1 of D with H-3 of F, H-1 of F with H-3 of G, H1 of G with H-2 of E and H-1 of E with H-2 of D, indicating the sequence D→F→G→E. In addition, the lack of any dipolar coupling between the signals of these resi-

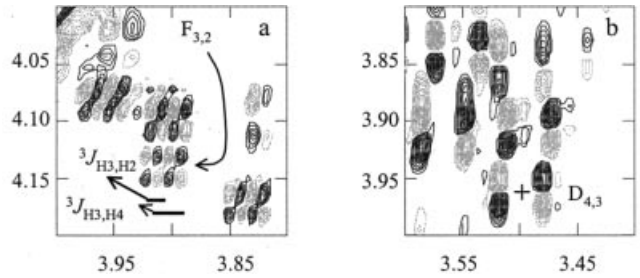

Figure 3. 500 MHz DQ-COSY spectrum of O-chain polysaccharide mixture: a) section of H-3/H-2 cross-peaks of rhamnose F residue, the active $^3J_{H3,H2}$ coupling generates antiphase densities whereas the passive $^3J_{H3,H4}$ one has the opposite behaviour; b) typical shape of the triplet of H-4 of the D unit, the cross points to the cross-peak centre, only boundaries densities are visible, the inner ones are cancelled by effect of the two coupling constants equivalence

dues with those of the other O-chain repeating unit is in agreement with the suggestion of two different O-chains. The low-field shift of the ^{13}C chemical-shift values of the glycosylated carbons confirmed the methylation data about the attachment points of glycosidic linkages and the NOE effects. The α-anomeric configuration for all residues was assigned on the basis of the up-field value of the ^{13}C chemical shift of the C-5 signal, in agreement with an α-configured rhamnose unit. In conclusion, the above data indicated the tetrasaccharide repeating unit:

2)-α-L-Rha*p*-(1→3)-α-L-Rha*p*-(1→3)-α-L-Rha*p*-(1→2)-α-L-Rha*p*-(1→

D **F** **G** **E**

Further support for this sequence was given by other diagnostic weak NOEs measured between the anomeric proton of each 2-linked rhamnose residue D and E with the H-5 proton of the previous unit, E and G, respectively, and the NOEs measured between the H-2 of the 3-linked rhamnose units F and G with the H-5 proton of the previous residues D and F, respectively. It is worthy to note that these NOEs are only compatible with the configurational dyad sequences α-L-α-L or α-D-α-D but not with the alternative combinations of anomeric and absolute configurations of the disaccharide moieties, which affect the conformation around the glycoside linkage and the inter-residual NOEs.[13] The above repeating unit is not new as it has al-

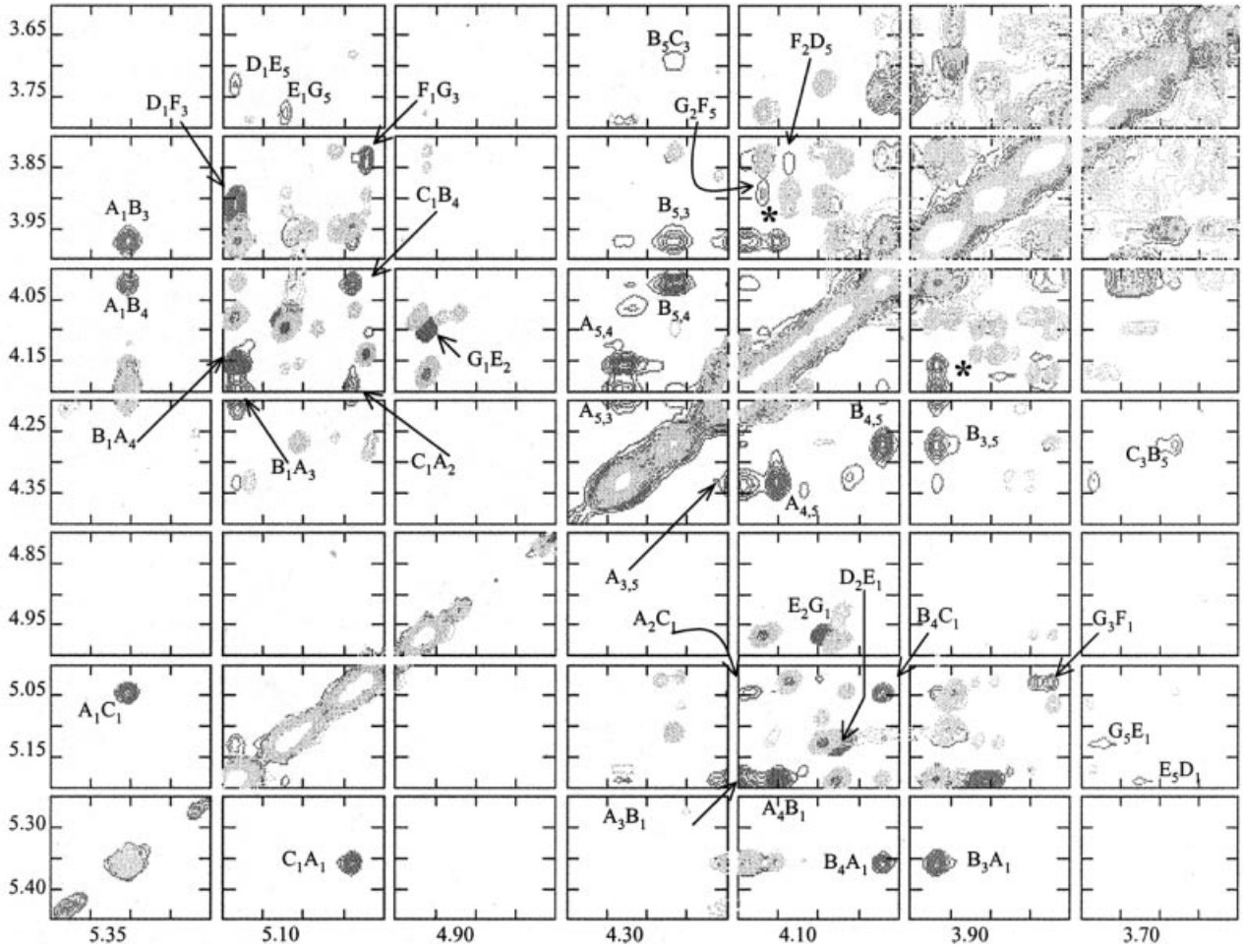

Figure 4. Overlay of TOCSY (light grey) and NOESY (grey) 2D NMR spectra, at 500 MHz, of the O-chain mixture (only NOE attributions are shown); the subscript numbers indicate the protons involved in the NOE connectivity of each residue; the star-labelled cross-peaks are due to the sum of more dipolar couplings (see text)

ready been found both in *Pseudomonas syringae* pvs. *Coronafaciens*[14] and as a minor component in *Pseudomonas syringae* pvs *garcae*.[15]

As far as the other O-chain was concerned, starting from the anomeric proton of the A residue it was possible to assign up to H-3 by scalar connectivity from the DQ-COSY spectrum. The signal of H-5 was then identified by exploiting its dipolar couplings with H-3 from the NOESY spectrum and its scalar coupling with the methyl group. Once H-5 had been found, the position of H-4 was clear as well, due to the strong dipolar coupling connectivity between these two protons; the NOE between H-3 and H-4 was not visible since it is too close to the diagonal of the spectrum.

The attribution of A to the 2,3-linked fucose residue was indicated by the ^{13}C chemical-shift values. In particular, glycosylation at C-2 is responsible for the high-field shift of the anomeric signal (δ = 92.5 ppm); the expected low-field shift of the C-2 signal is compensated by the neighbouring glycosylation at C-3. The NMR signal assignment of the fucose B residue was complicated by the coincidence of protons H-2 and H-3: the DQ-COSY spectrum correlated the anomeric signal of B with H-2 and no other correlation was present. The chemical-shift equivalence of H-2 and H-3 was evidenced in the HSQC spectrum, and this proton region was correlated to two carbons whose chemical shifts were in agreement with those expected for C-2 and C-3 of a 3-*O*-substituted fucose (see periodate degraded product data in Table 2). Once the H-3 proton of B had been identified, the assignment of H-4 and H-5 was performed as for the A residue. The NMR signal assignments of the C residue, identified as *t*-mannose was straightforward.

Table 2. ^{1}H and ^{13}C (italic) chemical shifts of the periodate-degraded O-chain **2** from *A. radiobacter* DSM 30147; data of methyl α-fucopyranoside are reported for comparison

	1	2	3	4	5	6
3-α-Fuc*p*	5.0	3.83	3.97	3.95	4.21	1.12
	98.8	*66.6*	*75.0*	*68.7*	*66.8*	*15.6*
α-Me-Fuc*p*	*100.5*	*69.0*	*70.6*	*72.9*	*67.5*	*16.5*

The α-configurations for both the fucoses A and B, and the mannose C residue were suggested on the basis of the low-field ^{1}H chemical-shift values of the anomeric signals: in the case of the fucose units they were supported by the small $^{3}J_{H1,H2}$ values and ^{13}C chemical shift of the anomeric signals; for the mannose unit the α-configuration was supported by the high-field C-5 and C-3 carbon chemical shifts.

The above data, together with those arising from the NOESY spectrum (discussed below), are in agreement with the methylation analysis and suggested the following repeating-unit structure for the other O-chain:

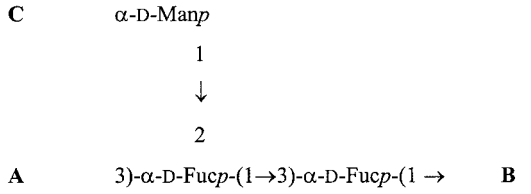

Information about the sequence of these residues were obtained by analysis of the NOESY spectrum; the complex NOE pattern was understood by comparing the experimental NOEs with those predicted by computer modelling (Table 3). Both fucose residues A and B show the expected inter-residual NOEs — H-1 of **B** has a stronger effect with H-4 than with H-3 of A and a similar pattern was found between H-1 of A and both H-3 and H-4 of B. However, in this case dipolar coupling with H-3 seems stronger than that with H-4, and, in addition, the attribution of the NOE effect with H-3 is complicated by the overlapping with H-2.

Table 3. Comparison of experimental distances (Å) of O-chain 2 with data derived from computer simulation; the subscript numbers indicate the protons involved in the NOE connectivity of each residue

Experimental NOEs	Experimental distances	Simulated distances
A_1B_3	2.61	2.52
A_1B_4	2.84	2.33
B_1A_3	2.67	2.71
B_1A_4	2.54	2.15
C_1A_1	2.42	2.14
C_1A_2	2.75	2.89
C_1B_4	2.73	2.73
$C_3B_5{}^{-1}$	2.88	2.32

Analysis of the NOEs from residue C was not straightforward due to the high number of dipolar couplings found in the spectrum. Its anomeric proton is correlated with H-1 (strong) and H-2 (medium) of residue A, and with H-4 (medium/strong) of B; in addition, a weak NOE between H-3 of C and H-5 of B is present as well. Clearly, all these NOEs are dictated by the conformation adopted by residue C respect to the fucose units in the backbone, and their comprehension is possible by modelling of the molecule. In the first part of this work the optimal dihedral angles were evaluated; when multiple minima were present, the lowest in energy was selected. For the first glycosidic junction — α-D-Man-(1→2)-α-D-Fuc — the following optimal angles were found: Φ = −61.9° and Ψ = −47.3° (see a in Figure 5) and for the second one — α-D-Fuc-(1→3)-α-D-Fuc — Φ = −54.3° and Ψ = −36.4° (see b in Figure 5). These dihedral angles were used for the construction of the following nonasaccharide unit:

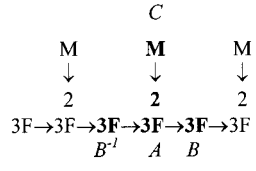

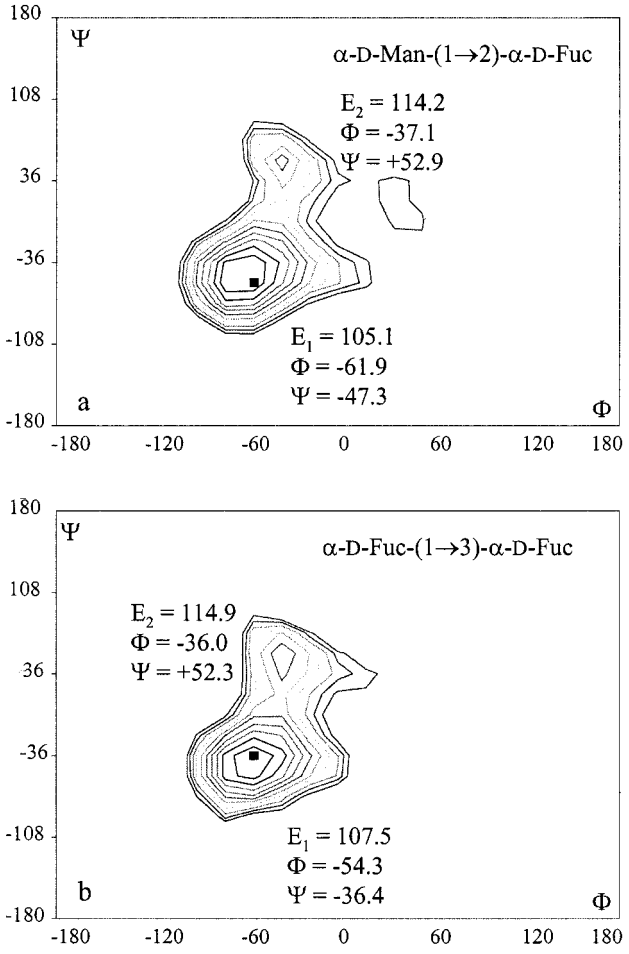

Figure 5. Relaxation maps for the glycosidic junction of: a) α-D-Man-(1→3)-α-D-Fuc and b) α-D-Fuc-(1→3)-α-D-Fuc; calculations were performed with the MM3 force field as implemented in MacroModel 8.0

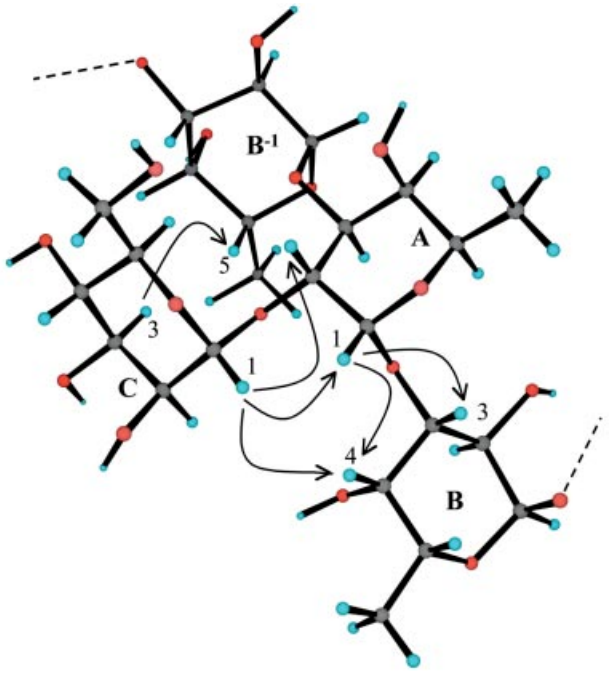

Figure 6. 3D model of the repeating unit of the second O-chain produced from *A. radiobacter* DSM 30147; the more relevant NOEs are indicated by arrows; fucose unit B^{-1}, belonging to another repeating unit, has been included in the picture in order to show one of the experimental NOEs

where M stands for α-D-Man, F for α-D-Fuc and the italic capital letters are the labelling of the sugar residues as shown in the ^{1}H NMR spectrum. All the sugar residues in bold are those for whom the simulated NOEs and averaged distances are calculated and reported in Table 3; these units are represented in Figure 6 as well. This starting structure was minimised and successively submitted to molecular dynamics analysis approximating the water solvent with the GB-SA model. The oligosaccharide was kept in a thermal bath at 303 K and its dynamic behaviour was observed as described in the Exp. Sect.

Ensemble average inter-proton distances for each molecule were extracted from dynamic simulations and translated into NOE contacts according to a full-matrix relaxation approach. The averaged distances were compared with those collected experimentally and showed a reasonable agreement. In more detail, all the NOE effects of residue C were understood and were compatible with the structure proposed. The preferred conformation of C places its anomeric proton much closer to H-1 than H-2 of A (Figure 6). Consequently, proton H-1 of C is located in the neighbourhood of H-4 of B as well, which in its preferred conformation is very close to H-1 of both C and A.

A careful examination of the nonasaccharide model led to the understanding of the NOE effect between H-3 of C and H-5 of B. This NOE arises between H-3 of the mannose unit and the H-5 of fucose residue B^{-1}, located backward from fucose A in the backbone sequence.

The NOEs indicated with a star in Figure 4 were understood after a careful study of the simulation data and are due to the sum of many small contributions. These dipolar couplings start from the coincident protons H-2 and H-3 of B and are connected to both H-3 and H-4 of A; looking at the simulation data, H-3 of B is expected to have a negligible effect with H-3 and H-4 of both the forward and backward residues A, and the same situation occurs for H-2 of B and the A protons. Summing all the small simulated densities for the pertinent protons, the theoretical cross peak between H-2/H-3 of B and H-3 of A (both the forward and the backward ones) appears as a medium/strong peak and that with proton H-4 of A as a peak of medium intensity, as found in the NOESY spectrum. The possibility that the NOEs indicated with a star could arise from spin-diffusion phenomena was excluded, since the spectrum itself does not contain any other suspicious and unexplainable NOEs.

The presence of two O-chains in the acid-hydrolysed LPS fraction was further supported by MALDI mass spectrometry. In this case, HPLC analysis by size-exclusion chromatography (SEC) was employed at an analytical level and for the preparation of MALDI samples. By this approach the chromatogram obtained by SEC on a TSKgel

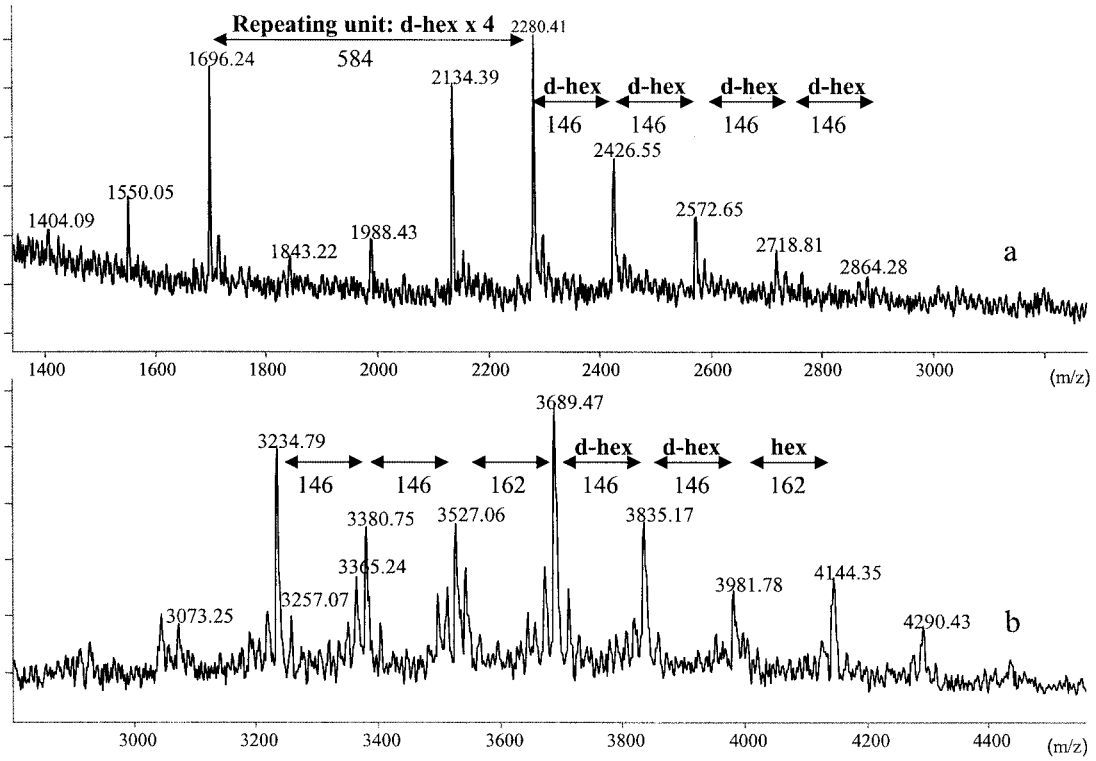

Figure 7. MALDI mass spectra of the more-representative fractions from TSKgel G3000 chromatography of the O-chain mixture: a) low molecular weight fraction of peak **1**, representative of O-chain **1**, b) chromatographic peak maximum of peak **2**, representative of O-chain **2**

G-3000, showed two peaks, **1** and **2**, each of which was further divided into different fractions. MALDI mass spectra were measured for all the fractions and the more representative results are reported in Figure 7. In the case of peak **1**, the MALDI spectrum of the chromatographic peak maximum shows a distribution of molecular ions centred at 5.500 Da, the difference between contiguous peaks corresponds to the loss of a water molecule and a deoxyhexose residue [m/z = 18 and m/z = 146 respectively (data not shown)]. No mass loss of a hexose residue is present. The MALDI spectrum (a in Figure 7) of a lower molecular mass fraction of the same chromatographic peak was more informative since two different molecular weight distributions were distinguishable: the first centred at m/z = 1696.2, and the second at m/z = 2280.4. As illustrated in Figure 7 (a), the mass difference between the two distributions is 584 Da, corresponding to a deoxyhexose tetrasaccharide. Inside each distribution, the difference between contiguous peaks is 146 Da, supporting the proposal that this O-chain is constituted by deoxyhexose residues only, in agreement with the proposed structure of O-chain **1**.

In the case of peak **2** (b in Figure 7), the MALDI spectrum of the chromatographic peak maximum shows a distribution of molecular ions centred at m/z = 3500 and mass differences corresponding to 146 and 162 Da, suggesting that the repeating unit of this second polysaccharide is a trisaccharide composed from two deoxyhexose and one hexose residues, in agreement with the structure of O-chain **2**.

Finally, in order to confirm the above conclusion, the purified LPS-3 fraction was degraded with sodium periodate. From chromatography of the crude reaction two main fractions were obtained, in agreement with the two O-chain structures proposed. The first contained an homopolysaccharide built up of 3)-α-D-Fuc*p*-(1→ units whose identification was easily obtained by NMR analyses (Table 2) and methylation data; the second fraction was identified by GC-MS analysis of the methylated derivative as the disaccharide α-L-Rha*p*-(1→3)-α-L-Rha*p*-(1→2)-Gro, as suggested by the diagnostic ions at m/z = 189 and 263 in the mass spectrum attributed to the oxonium cations of the terminal methylated rhamnose and the methylated disaccharide, respectively.

Experimental Section

***Agrobacterium radiobacter* and Bacterial Cultivation:** *A. radiobacter* strain DSM 30147 (type strain)[16] was grown at 27 °C in liquid shake culture (200 rpm) in Nutrient Broth (DIFCO) for 18 h (early stationary phase). The bacterial suspension was centrifuged (3500 g for 5 min) and the harvested cells were washed sequentially with 0.85% NaCl, ethanol, acetone and diethyl ether. Typically, 10 L of culture yielded 1.5 g of dry cells.

Isolation and Purification of the LPS Fraction: Dried cells were extracted according to the PCP method,[11] yielding LPS-1 fraction (3% g_{LPS}/g_{cells}). The pellet was further extracted according to the phenol-water method,[12] leading to the phenol extract LPS-2 (5%)

and to the water-fraction LPS-3 (7.5%). All phases were screened by 12% SDS-PAGE[17] on a miniprotean gel system from Bio-Rad; the samples (4 μg) were run at constant voltage (150 V) and stained according to the procedure of Kittelberger.[18] High molecular weight lipopolysaccharide material was found in the water phase and in the PCP extract.

The LPS-3 fraction (50 mg) was further purified of nucleic material and low molecular weight glucane on Sephacryl HR 400 (Pharmacia, 1.5 × 90 cm, eluent NH_4HCO_3 50 mM, flow 0.4 mL/min). The eluate was monitored with an R.I. refractometer (K-2310 Knauer) and the collected peaks screened again with SDS-PAGE, leading to 15 mg (2.3% yield respect dry cells) of the LPS-2 fraction.

Chemical Composition Analysis: Monosaccharides were analysed as acetylated *O*-methyl glycoside derivatives and lipids as methyl esters, as reported previously.[6]

The absolute configuration was determined by analysis of the chiral 2-octyl derivatives according to the procedure of Leontein.[19]

Glycosyl-linkage analysis of LPS was performed according to the procedure of Sandford,[20] the permethylated lipopolysaccharide was recovered in the organic layer of the water/chloroform extraction and converted into its partially methylated alditol acetates.[21] GC-MS analysis conditions for all the derivatives mentioned above were the same and were acquired on an Agilent 5973 instrument, using a SPB-5 capillary column (Supelco, 30 m × 0.25 i.d.; flow rate, 0.8 mL/min; He as carrier gas), with the temperature program: 150 °C for 5 min, 150 → 300 °C at 5.0 °C/min, 300 °C for 15 min. Mass spectra were recorded at an ionisation energy of 70 eV and an ionising current of 0.2 mA.

Isolation of the O-Specific Polysaccharide Fraction: Purified LPS-3 fraction (10 mg) was dissolved in 1% acetic acid solution (2 mL), and kept at 100 °C for 2 h. After cooling, the solution was centrifuged at 6000 rpm for 20 min and the clear supernatant freeze-dried. The O-chain was purified by GFC on Sephacryl HR 100 (Pharmacia, 1.5 × 70 cm, NH_4HCO_3 50 mM, flow 0.4 mL/min, Figure 1), and the eluate monitored by refractive index as mentioned above. The O-chain was isolated in approx. 60% yield from LPS.

Smith Degradation Product of the O-Chain: Periodate-degraded product was obtained from the O-chain according to a procedure reported in the literature.[22]

NMR Spectra Acquisition: 2D NMR experiments were carried out on a Varian Inova 500 of Consortium INCA (L488/92, Cluster 11), equipped with a reverse probe operating at 25 °C. Chemical shifts of spectra recorded in D_2O are expressed in δ relative to internal acetone (δ = 2.225 and 31.4 ppm for ^1H and ^{13}C, respectively). Two dimensional spectra (DQ-COSY, TOCSY, NOESY gradient-HSQC) were measured using the standard Varian software.

For the homonuclear experiment, 512 FIDs of 2048 complex data points were collected, with 40 scans per FID. The spectral width was set to 10 ppm and the frequency carrier was placed at the residual HOD peak. For the HSQC spectrum, 256 FIDS of 2048 complex points were acquired with 50 scans per FID, the GARP sequence was used for ^{13}C decoupling during acquisition. Conversion of the Varian data and processing was performed with standard Bruker Xwin NMR 1.3 program; the spectra were assigned using the computer program Pronto.[23]

Molecular Mechanics and Dynamics Calculations: Molecular Mechanic and Dynamics calculations were performed using the MM3* force field as implemented in MacroModel 8.0, installed under the Red Hat 8 operating system. The MM3* force field used[24] differs from the regular MM3 force field in the treatment of the electrostatic term, since it uses charge−charge instead of dipole−dipole interactions. A molecular mechanics approach has been used to evaluate the optimal dihedral angles (Table 3) for each glycosidic junction; the calculations were performed for a dielectric constant, ε, of 80, as an approximation for bulk water. Relaxed energy maps were calculated employing the DRIV utility (modulated with the DEBG option 150, which causes the program to start each incremental minimization reading the initial input structure file). For each disaccharide entity, both Φ and Ψ were varied incrementally using a grid step of 18°, each (Φ, Ψ) point of the map was optimized using 2000 P.R. conjugate gradients, Φ is defined as $H_1-C_1-O-C_{aglycon}$ and Ψ as $C_1-O-C_{aglycon}-H_{aglycon}$. The plotting and the analysis of the relaxed surfaces was performed with the 2D-plot facility built in the MacroModel package, the two adiabatic maps are shown in Figure 5. On the basis of the values obtained, the selected oligosaccharide was built employing the optimal dihedral angles found (when two minima were present, the lowest in energy was considered), and minimized again with the MM3* force field, but approximating water solvent using the GB/SA model. The molecular dynamics simulation started from this optimized structure, subjected initially to an equilibration time of 200 ps, and successively kept in a thermal bath at 303 K for 8000 ps, a dynamic time-step of 1.5 fs together with the SHAKE protocol was applied to the hydrogen bonds, and coordinates were saved every 4 ps of simulation leading to the collection of 2000 structures. Ensemble average-distances between mentioned inter-residue proton pairs were calculated from the dynamic simulation employing the following two programs: NOEPROM[25] (NOEs simulations and coordinates extraction) and ORIGIN.

MALDI-MS Analysis: MALDI-TOF analyses were conducted both in linear and in reflector mode using an Applied Biosystems (Framingham, MA, USA) Voyager STR instrument equipped with delayed-extraction technology. Ions formed by a pulsed UV laser beam (nitrogen laser, λ = 337 nm) were accelerated through 24 kV. In order to better determine the MW distribution of the O-chain polysaccharide,[26] 300 μg of the sample was size fractionated on a size exclusion chromatography (SEC) system consisting of a Waters 515 HPLC pump, a TosoHaas TSKgel G3000 PWXL column (7.8 mm × 30 cm, Tosoh Biosep GmbH) and a Waters 410 differential refractometer as detector. Microfractions obtained with H_2O as eluent at a flow rate of 0.8 mL/min, were collected every 12 s and subsequently dried on a centrifugal concentrator (SpeedVac Thermo Savant − USA). Selected fractions of the chromatographic peak were finally diluted in 20 μL of 0.1% CF_3CO_2H and mixed in a 1:10 ratio with the matrix solution (recrystallized 2,5-dihydroxybenzoic acid 30 g/L in 0.1% CF_3CO_2H/acetonitrile, 80:20) before recording the spectra in the negative mode.

Acknowledgments

The authors thank the "Centro di Metodologie Chimico-Fisiche" of the University Federico II of Naples for the facilities offered by the Computer Modelling and NMR sections, and MIUR for financial support (M. P. Progetti di Ricerca di Interesse Nazionale, 2002 Roma).

[1] D. C. Sigee, *Bacterial Plant Pathology: Cell and Molecular Aspects*, Cambridge University Press, **1993**.
[2] M. H. Ryder, D. A. Jones, *Biological Control of Crown Gall* in, *Biological Control of Soil-borne Plant Pathogens*, (Ed.: D. Hornby), CAB International, Wallingford, **1990**, 45−63.
[3] U. Zahringer, B. Linder, E. T. Rietschel, *Adv. Carbohydr. Chem. Biochem.* **1994**, *50*, 211−276.

[4] H. Brade, S. M. Opal, S. N. Vogel, D. C. Morrison, *Endotoxins in Health and Disease*, Marcel Dekker Inc., New York, Basel, **1999**.

[5] C. De Castro, E. Bedini, R. Nunziata, R. Rinaldi, L. Mangoni, M. Parrilli, *Carbohydr. Res.* **2003**, *338*, 1891−1894.

[6] C. De Castro, O. De Castro, A. Molinaro, M. Parrilli, *Eur. J. Biochem.* **2002**, *269*, 2885−2888.

[7] A. Molinaro, C. De Castro, R. Lanzetta, M. Parrilli, A. Raio, A. Zoina, *Carbohydr. Res.* **2003**, *338*, 2721−2730.

[8] C. De Castro, L. Sturiale, M. Parrilli, *Eur. J. Org. Chem.* **2004**, 2436−2440.

[9] L. R Evans, A. Linker, G. Impallomeni, *Int. J. Biol. Macromol.* **2000**, *27*, 319−326.

[10] W. M.. Dunne Jr, J. Tilman, J. C. Murray, *J. Clin. Microbiol.* **1993**, *31*, 2541−2543.

[11] C. Galanos; O. Luderitz; O. Westphal, *Eur. J. Biochem.* **1969**, *9*, 245−249.

[12] O. Westphal, K. Jann, *Methods Carbohydr. Chem.* **1965**, *5*, 83−91.

[13] G. M. Lipkind, A. S: Shashkov, S. S. Mamyan, N. K. Kochetkov, *Carbohydr. Res.* **1988**, *181*, 1−12.

[14] E. L. Zdorovenko, G. V. Zatonsky, G. M. Zdorovenko, L. A. Pasichnyk, A. S. Shashkov, Y. A. Knirel, *Carbohydr. Res.* **2001**, *336*, 329−336.

[15] M. M. Corsaro, C. De Castro, A. Molinaro, M. Parrilli, *Recent Res. Devel. Phytochem.* **2001**, *5*, 119−138.

[16] B. Holmes, P. Roberts, *J. Appl. Bacteriol.* **1981**, *50*, 443−467.

[17] U. K. Laemmli, *Nature (London)* **1970**, *97*, 620−628.

[18] R. Kittelberger, F. Hilbink, *J. Biochem. Biophys. Methods* **1993**, *26*, 81−86.

[19] K. Leontein, B. Lindberg, J. Lonngren, *Carbohydr. Res.* **1978**, *62*, 359−362.

[20] P. A. Sandford, H. E. Conrad, *Biochemistry* **1966**, *5*, 1508−1517.

[21] P. Albersheim, D. J. Nevins, P. D. English, A. Karr, *Carbohydr. Res.* **1967**, *5*, 340−345.

[22] G. W. Hay, B. A. Lewis, F. Smith, *Methods Carbohydr. Chem.* **1965**, *5*, 357−61.

[23] M. Kjaer, K. V. Andersen, F. M. Poulsen, *Methods Enzymol.* **1994**, *239*, 288−308.

[24] N. L. Allinger, Y. H. Yuh, J. H. Lii, *J. Am. Chem. Soc.* **1989**, *111*, 8551−8566.

[25] J. L. Asensio, J. Jiménez-Barbero, *Biopolymers* **1995**, *35*, 55−75.

[26] D. Garozzo, G. Impallomeni, E. Spina, L. Sturiale, F. Zanetti, *Rapid Commun. Mass Spectrom.* **1995**, *9*, 937−41.

Received April 7, 2004

